# Parallel ion compressibility effects on kinetic ballooning mode for different magnetic shears

Y. Li and Y. Xiao[a)]
*Institute for Fusion Theory and Simulation, Department of Physics, Zhejiang University, Hangzhou 310027, People's Republic of China*

(Received 19 December 2016; accepted 24 April 2017; published online 10 August 2017)

Various gyrokinetic simulations suggest that the kinetic ballooning mode (KBM) instability is sensitive to the numerical implementation of equilibrium magnetic configuration in tokamaks. In this work, the gyrokinetic code GTC is employed to investigate the KBM's sensitivity to equilibrium plasma profiles. An outward radial shift of the radial mode is found for the normal magnetic shear case, but there is no shift if the shear is negative. The simulation results are explained by a linear eigenmode theory. It is found that the observed phenomenon is an effect of the parallel ion compressibility. *Published by AIP Publishing.*
[http://dx.doi.org/10.1063/1.4997489]

## I. INTRODUCTION

The ideal MHD ballooning mode (IBM) in tokamak plasmas is one of the most thoroughly investigated MHD instabilities. It imposes an upper limit for the maximum pressure gradient in the first IBM stability regime and suggests the existence of a second stability regime arising from the Shafranov shift of the magnetic axis when the plasma pressure gradient is sufficiently high. A closely related mode is the kinetic ballooning mode (KBM), which includes important kinetic modifications to the IBM, e.g., the diamagnetic flow, finite Larmor radius effect, and wave particle resonance. The KBM physics has been investigated for many years[1,2] and its physics is still not fully clear. Earlier efforts have been focused on the low-beta, large-aspect-ratio s-$\alpha$ equilibrium model,[3] under the assumptions $\omega \gg k_{||} v_{Ti}$ and $\omega \ll \omega_{*e}$, where $\omega$ is the characteristic frequency of KBM, $k_{||}$ represents the parallel wave number, $v_{Ti}$ is the ion thermal speed, and $\omega_{*e}$ is the electron diamagnetic frequency.[4] Subsequent works have included the effects of trapped electrons, passing ions, parallel magnetic perturbation, and so on. The stability of the KBM has been investigated in the parameter regimes relevant to internal transport barriers (ITB) with negative magnetic shear.[5,6]

Even after one decade of gyrokinetic simulation of KBM,[7–10] detailed understanding and verification between different codes still remain challenging. Recently, the properties of the linear KBM predicted by different gyrokinetic codes, such as GS2,[11] GTC,[7] GYRO,[12] and GENE,[13] have been compared.[14] It is realized that the linear KBM, in contrast to the electrostatic modes such as ion temperature gradient (ITG) mode and trapped electron mode (TEM), is extremely sensitive to the equilibrium magnetic configurations implemented in the different codes.[14]

In this work, we carry out the KBM simulations using the GTC code. It is found that both linear growth rate and real frequency depend on the width of the gradient profile, i.e., effectively the simulation window implemented in the code. In particular, the radial mode structure suffers an outward shift in the normal magnetic shear (i.e., the shear monotonically increases with $r$, or the poloidal flux $\psi_p$) case, but there is no shift in the reversed-shear case. We also propose an eigenmode theory that explains this shear-dependent radial mode shift. The parallel ion compressibility is found to be responsible for the radial mode shift observed in the simulation.

In Sec. II, we carry out KBM simulations using the GTC code and find the locality of the plasma profile which has a strong effect on the linear KBM properties. In Sec. III, we develop an eigenmode theory and numerically solve the eigenvalue problem to study the linear KBM physics. In Sec. IV, we show that the parallel ion compressibility has a stabilizing effect on the KBM for normal shear, which is responsible for the radially outward shift of the KBM mode structure. In Sec. V, we show that, depending on the magnetic shear, the parallel ion compressibility can have quite different effects on the KBM. In Sec. VI, the relationship between the magnetic shear effect and the parallel ion compressibility effect is verified by the GTC simulation. Section VII gives the conclusion and discussion.

## II. PLASMA PROFILE EFFECT ON THE KBM

As mentioned, the KBM is extremely sensitive to the numerical implementation of the equilibrium magnetic configuration.[14] Here, we use the GTC code[15–19] to study the KBM sensitivity to the numerical implementation of the plasma density and temperature profiles. The GTC code is a global particle-in-cell (PIC) gyrokinetic code which can directly import experimental magnetic equilibrium and profiles as the simulation setup. In order to investigate the numerical plasma profile effect on the KBM instability, analytical flat gradient profiles for the density and temperature have been used in the simulation as a reference local model for the plasma profile, as shown in Figs. 2(b)–2(d) by the dashed lines. The q profile used in the GTC simulations is

[a)]Author to whom correspondence should be addressed: yxiao@zju.edu.cn

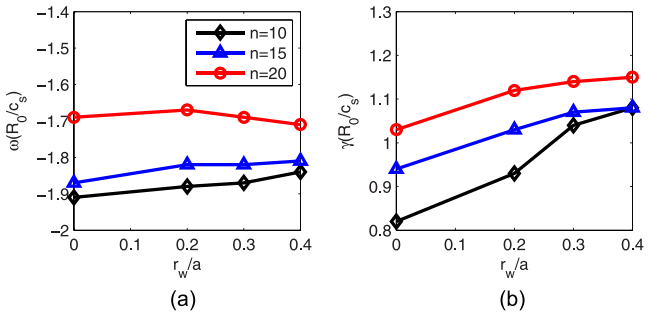


FIG. 1. The frequency and the growth rate of $n = 10, 15, 20$ modes as a function of the profile width $r_w/a$ (from the GTC simulation).

$q(\psi_p) = q_1 + q_2\left(\frac{\psi_p}{\psi_w}\right) + q_3\left(\frac{\psi_p}{\psi_w}\right)^2$, where q is the safety factor, $\psi_p$ is the poloidal flux, $\psi_w$ is the poloidal flux on the wall, $q_1 = 0.81$, $q_2 = 1.1$, and $q_3 = 1.0$. The local (flat gradient) plasma density and temperature profiles are generally used by the global simulations for verifying the corresponding local theory or the simulation results from the local codes. In the GTC simulation, the temperature and density gradient profiles are assumed to be flat in the central region of the radial domain, namely, $L_n^{-1}, L_T^{-1} \propto \exp\left[-\left(\frac{r-0.5a}{r_w}\right)^6\right]$, where $a$ is the minor radius, $r_w$ represents the width of the flat region for the gradients, and $L_n^{-1} = -d\ln n/dr$, $L_T^{-1} = -d\ln T/dr$ are the scale lengths of density and temperature, respectively.

Figure 1 shows the simulation results for three typical toroidal mode numbers, and the simulation parameters evaluated at $r = a/2$ are $\beta = 2.0\%$, $\varepsilon = a/R = 0.35$, $k_\theta\rho_s = 0.2$ and $q = 1.4$, $s = 0.81$, $\alpha = 0.73$, $R/L_n = 2.2$, $R/L_T = 7.0$, where $s = d\ln q/d\ln r$ is the magnetic shear, $\beta = \frac{8\pi n T_e}{B^2}$ is the ratio of the plasma pressure of electron to the magnetic pressure, $\alpha = \frac{2q^2R}{L_n}\beta(1+\eta)$, where $\eta = L_n/L_T$ is the ratio of the temperature gradient to the density gradient. One can clearly see that the KBM linear frequency and the growth rate are sensitive to the width of the local profile $r_w$. In Fig. 1, the point $r_w = 0$ corresponds to a global analytic profile for the temperature and density, as shown by the dashed line in Fig. 2(a), where only the peak gradient at $r = a/2$ is the same as the other three local profiles. Both linear frequency and the growth rate in Fig. 1 are measured at $r = 0.5a$. The linear frequency depends weakly on the width of the local profile $r_w$. The linear growth rate depends much more strongly on $r_w$. It is also found that the dependence is more pronounced for smaller toroidal mode numbers, as shown in Fig. 1(b).

Figure 2 shows the GTC simulation results for the radial mode structure for different widths of the temperature and density gradient profiles. The toroidal mode number is $n = 10$, and the peak positions correspond to that of the mode rational surfaces for different poloidal mode numbers. The simulation range of the poloidal magnetic flux $\psi_p$ is $(0.02\psi_w, 0.88\psi_w)$, where $\psi_w$ is the magnetic flux at the wall, and the homogeneous Dirichlet boundary conditions is used for perturbed quantities in the simulation. Since the radial width of each individual mode is much narrower than the radial range of the simulation, the boundary effect is negligibly small. We can see that the radial mode structure moves

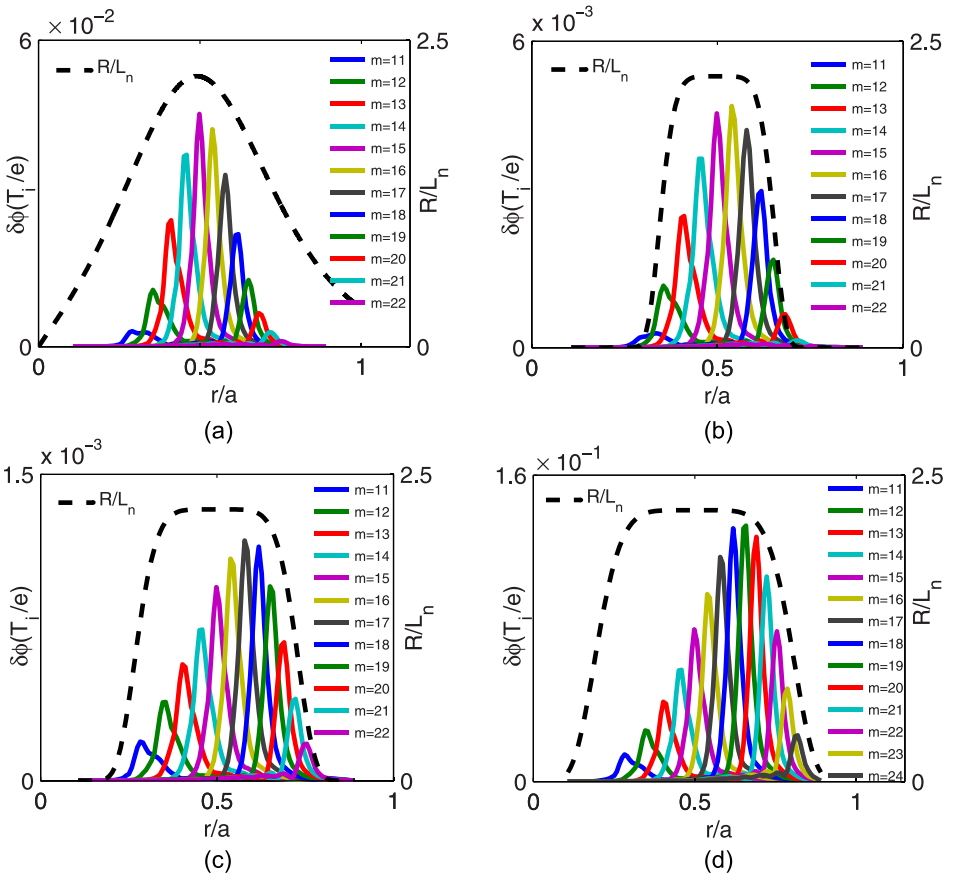


FIG. 2. Radial mode structure of KBM with mode number n = 10 and different mode numbers m (blue solid curves) for different density/temperature gradient profiles: (a) global profile, (b) $r_w = 0.2a$, (c) $r_w = 0.3a$, and (d) $r_w = 0.4a$.

outward as the gradient width $r_w$ increases. It is therefore of interest to find out the cause of this outward shift.

## III. LINEAR BALLOONING THEORY WITH PARALLEL ION COMPRESSIBILITY

In this section, we give the theoretical basis for parallel ion compressibility, and the physics explanation of the effect of parallel ion compressibility is provided in Sec. IV. Using the ballooning representation and s-α model,[3] we can write the normalized eigenmode equation for the KBM[4,6]

$$\frac{\partial}{\partial\theta}\left[1+(s\theta-\alpha\sin\theta)^2\right]\frac{\partial\delta\Psi}{\partial\theta}+\frac{\alpha}{4\varepsilon_n(1+\eta)}\times\left[(\Omega-1)\left(\Omega-f(\theta)\right)+\eta_e f(\theta)-\frac{(\Omega-1)^2}{1+\tau-\tau I}+\tau\frac{\partial}{\partial\theta}H\frac{\partial}{\partial\theta}\right]\delta\Psi=0, \tag{1}$$

where the parallel ion compressibility is retained in the last term, related to the lowest order of the parallel ion current, $\theta$ is the ballooning angle with respect to the field line, $q$ is the safety factor, $\tau=T_e/T_i$ is the electron/ion temperature ratio, $\varepsilon_n=L_n/R$ is the inverse of the normalized density gradient, $\eta_e=d\ln T_e/d\ln n_e$ and $\Omega=\omega/\omega_{*e}$ is the mode frequency normalized by the electron diamagnetic frequency $\omega_{*e}=\frac{k_\theta cT_e}{eBL_n}$, and $\delta\Psi$ is the perturbed field which is an even function of $\theta$. The functions $f(\theta)$, $I$, and $H$ are defined by

$$f(\theta)=2\varepsilon_n[\cos\theta+(s\theta-\alpha\sin\theta)\sin\theta], \tag{2}$$

$$I=\left\langle\frac{\omega-\hat{\omega}_{*i}}{\omega-\hat{\omega}_{di}}F_iJ_0^2(\Lambda_i)\right\rangle_v, \tag{3}$$

$$H=\frac{1}{\omega_{*e}^2q^2R^2}\left\langle\frac{\omega-\hat{\omega}_{*i}}{\omega-\hat{\omega}_{di}}v_{||}^2F_iJ_0^2(\Lambda_i)\right\rangle_v, \tag{4}$$

where $\Lambda_i$, $\hat{\omega}_{*i}$, and $\hat{\omega}_{di}$ can be expressed as

$$\Lambda_i=\sqrt{2}k_\theta\rho_i\sqrt{1+(s\theta-\alpha\sin\theta)^2}\,v_\perp/v_T, \tag{5}$$

$$\hat{\omega}_{*i}=-\frac{\omega_{*e}}{\tau}\left[1+\eta_i\left(\frac{m_iv_{||}^2+m_iv_\perp^2}{2T_i}-\frac{3}{2}\right)\right], \tag{6}$$

$$\hat{\omega}_{di}=-\frac{\omega_{*e}}{\tau}f(\theta)\left(\frac{m_iv_{||}^2}{2T_i}+\frac{m_iv_\perp^2}{4T_i}\right). \tag{7}$$

Here, $F_i$ is the Maxwellian distribution function for the ions, $v_T=\sqrt{2T_i/m_i}$ is the ion thermal velocity, $\rho_i=\frac{v_T}{\omega_{ci}}=\frac{v_Tm_ic}{eB}$ is the Larmor radius of ion, $J_0$ is the zeroth order Bessel function, and $\langle\cdots\rangle_v$ denotes the velocity space integral. For simplicity, we assume $\tau=T_e/T_i=1$ and $\eta=\eta_e=\eta_i$. Note that the parallel ion compressibility, essentially given by the term containing $H$ in Eq. (1), is inversely proportional to $q^2$.

To solve Eq. (1), a numerical nonlinear eigenvalue code is developed to find the eigenvalue, i.e., the normalized frequency Ω. The perturbed field $\delta\Psi$ is then represented by a discrete vector, and thus Eq. (1) could be transformed to a matrix form. The resulting discrete nonlinear eigenmode equation can be solved iteratively. The integral $I(\theta)$ and $H(\theta)$ are related to the standard plasma dispersion relation function

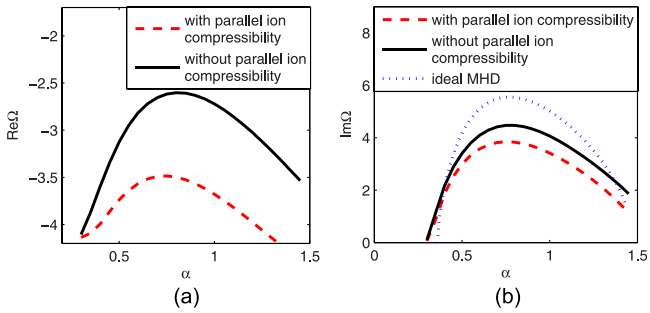


FIG. 3. The frequency and growth rate vs. α for cases with or without the parallel ion compressibility (red dashed and the black solid curves, respectively) and of the ideal MHD ballooning mode (blue dotted curve).

$$Z(\zeta)=\int\frac{\exp(-z^2)}{z-\zeta}dz, \tag{8}$$

which can be expressed in terms of the complex error function, and the complex error function can be evaluated accurately and rapidly by using the basis function method and the Fast Fourier Transformation (FFT).[20,21]

## IV. EFFECT OF PARALLEL ION COMPRESSIBILITY

In order to show the effect of the parallel ion compressibility, we use the analytic theory to compare the KBM results for with or without the parallel ion compressibility. Figure 3 shows the resulting growth rates and real frequencies, calculated by the analytic theory illustrated in Section III, normalized by the electron diamagnetic frequency $\omega_{*e}$ for: $s=0.4$, $b_0=(k_\theta\rho_i)^2=0.01$, $\eta=2$, $q=2$, and $\varepsilon_n=0.175$. Figure 3 also shows that the parallel ion compressibility provides a stabilizing effect that reduces the growth rate of the KBM in the IBM (ideal MHD ballooning mode) unstable regime.

Figure 4 shows the eigenfunction along the parallel direction calculated by analytic theory for the cases with or without the parallel ion compressibility, where only half the eigenfunction is shown since the mode structures are even in $\theta$. The value of the perturbed field at $\theta=0$ is set to unity for simplicity, and the simulation parameters are the same as in Fig. 3. In the MHD unstable region, the eigenfunction is confined around the outside middle plane with $\theta=0$. We also note that the most unstable region is around that with the bad curvature, or $\theta=0,2\pi,4\pi,\ldots$, and the least unstable region is around that with the good curvature, or $\theta=\pi,3\pi,\ldots$, which is consistent with the ballooning assumption of the theory. The parallel ion compressibility can broaden the mode structure, i.e., more perturbed field energy moves away from the most unstable ballooning angles, which means the perturbed energy moves away from the bad curvature region, thereby leading to stabilization by the parallel ion compressibility.

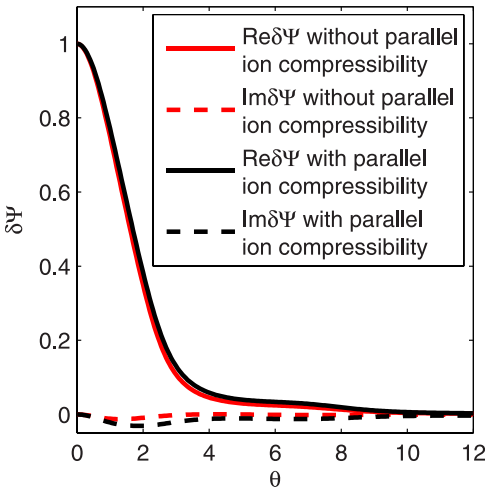


FIG. 4. Comparison of eigenmode structure with or without parallel ion compressibility in the ballooning space, with $\alpha = 0.8$.

As mentioned, the parallel ion compressibility term is inversely proportional to the square of the safety factor and it can stabilize the KBM. The safety factor profile used here has normal shear. At larger radial position, the safety factor $q$ is larger, and the stabilization effect from the parallel ion compressibility becomes weaker. Thus, the growth rate of the linear eigenmode increases in the radially outward direction, which induces the outward shift of the radial mode structure in Fig. 2.

In the GTC linear simulation, one particular toroidal mode number n is selected for the stability analysis with multiple poloidal modes coexisting. Therefore, the growth rate at $r = 0.5a$ is enhanced by the coupling with the outside poloidal mode which grows faster due to the less stabilizing effect from the parallel ion compressibility. The smaller n mode has a stronger poloidal mode coupling with the neighboring mode. Thus, the dependence is more pronounced for smaller toroidal mode numbers in Fig. 1(b).

## V. MAGNETIC SHEAR EFFECT ON THE KBM

In Sec. IV, we have studied the effect of the parallel ion compressibility under the normal shear. It has also been found that the KBM will be unstable due to the interchange drive when magnetic shear is small and pressure gradient is sufficiently small.[5] In this section, we examine the KBM mode structure with reversed magnetic shear. The q profile in our GTC simulation[22] is a parabolic function of $r$, or $q(r) = q_{mid} + c(r/a - 0.5)^2$. So, the magnetic shear increases monotonically with $r$ and poloidal flux $\psi_p$ near $r = a/2$, where $s = 0$ and $q = q_{mid}$ at $r = a/2$. The density and temperature gradient profile are still the flat profile with $r_w = 0.3$. The GTC simulation result is shown in Fig. 5, for $\beta = 2.0\%$, $\alpha = 0.73$, $k_\theta \rho_s = 0.2$, $n = 10$, and $q = 1.4$, $R/L_n = 2.2$, $R/L_T = 7.0$ at $r = a/2$, with the q profile given by $q_{mid} = 1.4$ and $c = 4.0$. Consistent with previous studies,[6] the linear mode from the GTC simulation is mostly unstable around $r = 0.5a$, where the magnetic shear $s$ is very small and the growth rate is much larger than that in other radial positions, as can be seen in Fig. 5.

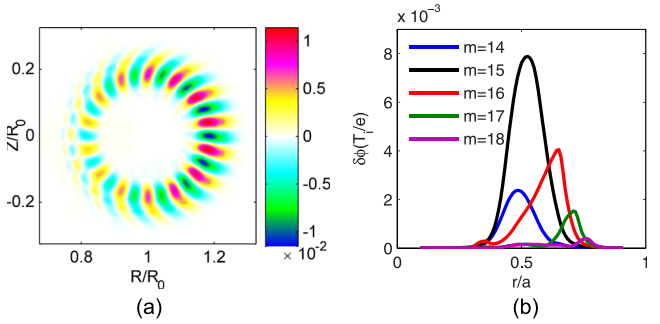


FIG. 5. (a) Mode structure with $n = 10$ in the poloidal plane and (b) the radial mode structure for different mode numbers m obtained by the GTC simulation for a reversed shear configuration.

Our eigenvalue solver can also be used to investigate the magnetic shear effect on the KBM for cases with and without the parallel ion compressibility. Figure 6 shows the result for $\alpha = 0.35$, $k_\theta^2 \rho_s^2 = 0.01$, $\eta_e = \eta_i = 2$, $L_n/R = 0.175$, and $q = 2$. Because the s-$\alpha$ model does not include average good curvature effect, strictly it is not valid for zero shear; thus, there is no result at $s = 0$. It is found that the linear frequency and the growth rate are strongly affected by the magnetic shear. When the parallel ion compressibility is ignored, the growth rate increases rapidly with s when $s < 0$, and decreases relatively slowly for $s > 0$. This result is consistent with that from our GTC simulation in Fig. 5, where the radial mode structure is restrained around the zero-shear point. The growth rate of the unstable poloidal mode increases sharply for $s < 0$, and decreases slowly for $s > 0$. We also note that the stabilizing effect of the negative shear is consistent with the results from the MHD energy principle.[23,24]

## VI. EFFECT OF PARALLEL ION COMPRESSIBILITY FOR DIFFERENT MAGNETIC SHEARS

In this section, we discuss the effect of parallel ion compressibility for different magnetic shears. Figure 6 also shows that in the positive shear region, the parallel ion compressibility can provide stability for the KBM, but it does not affect the linear frequency and the growth rate in the negative shear region. To verify this phenomenon, we consider two different q profiles for our GTC simulation, which have constant positive and negative shears in the central region of the simulation domain. Setting $q\left(\frac{a}{2}\right) = 1.4$ and using the relationship $s = \frac{r}{q}\frac{dq}{dr}$, we can obtain the q profile from the magnetic shear profile $s(r)$:

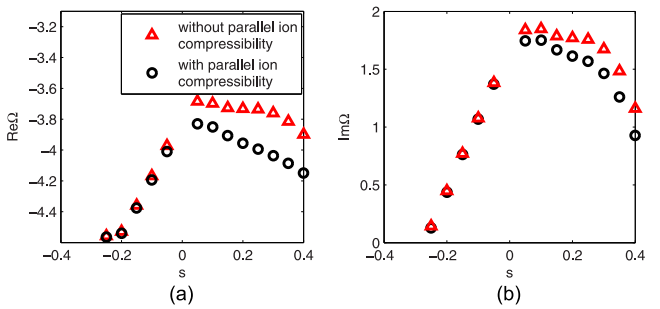


FIG. 6. Dependence of the frequency and growth rate on the magnetic shear $s$ for with or without parallel ion compressibility.

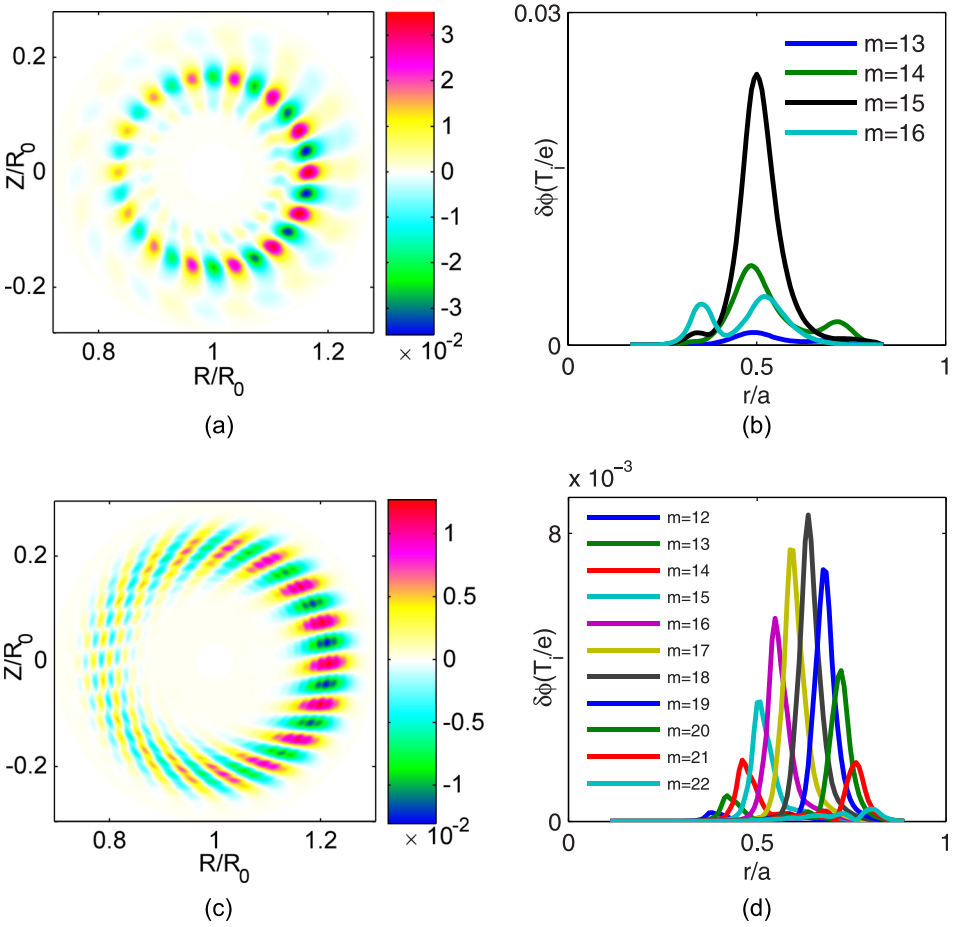


FIG. 7. Mode structure with $n = 10$ in the poloidal plane and the radial mode structure for different mode numbers m with (a) and (b) $s_{mid} = -0.2$, (c) and (d) $s_{mid} = 0.81$.

$$s(r) = \begin{cases} -\dfrac{s_{mid}}{r_l^2}(r - r_l)^2 + s_{mid} & 0 < r < r_l \\ s_{mid} & r_l < r < r_r \\ \dfrac{s_{\max} - s_{mid}}{(a - r_r)^2}(r - r_r)^2 + s_{mid} & r_r < r < a, \end{cases} \quad (9)$$

where $s_{mid}$ is the constant magnetic shear in the central region for simulating the local limit, $r_l < r < r_r$, with $r_l + r_r = a$, and $r_r - r_l = r_w$ indicates the width of local profile, $s_{\max}$ is the magnetic shear at $r = a$ position. The density and temperature gradient profiles are still the local profile used earlier. To show the parallel ion compressibility effects with positive and negative shears, the GTC simulation is carried out for $s_{mid} = 0.81$ and $s_{mid} = -0.2$, respectively, with the other parameters in Sec. V unchanged.

As shown in the Figs. 7(c) and 7(d), the radial mode structure stays centered at $r = a/2$ for the negative shear case, but it moves outward for the positive shear case. The different behaviors of the KBM mode structure for different magnetic shears are fully consistent with that predicted by the theory given in the last section, namely, the parallel ion compressibility provides stability for the KBM mode for $s > 0$, and it does not affect the KBM stability when $s < 0$.

## VII. CONCLUSION AND DISCUSSION

In this work, we have investigated the KBM instability using the gyrokinetic simulation code GTC. We found that the linear growth rate and frequency are affected by the width of the local profile. The poloidal mode structure moves outward in the radial direction for the normal magnetic shear, whereas it does not move for the negative magnetic shear. A linear eigen mode theory is proposed to explain this radial shift of the KBM. It is found that the parallel ion compressibility, ignored in the existing theories,[4] affects the growth rate differently for positive and negative shears. For positive magnetic shear, it provides stability to the KBM and decreases its growth rate. However, for negative magnetic shear, it does not affect the growth rate at all. These theoretical results can be explained qualitatively by the GTC simulation results. We also note that the theory used here to analyze the KBM is a local one. To interpret the simulation results more quantitatively, the next-order radial envelope analysis should be invoked, which we leave for the future work.

## ACKNOWLEDGMENTS

This work was supported by National Magnetic Confinement Fusion Energy Research Program under Grant Nos. 2015GB110000, 2013GB111000, China NSFC under Grant No. 11575158, the Recruitment Program of Global Youth Experts. Y. Li would like to thank H. S. Xie, H. T. Chen, and W. Chen for the useful discussions. Y. Xiao is grateful for the helpful discussions with Professor Z. Lin and L. Chen.

[1]W. M. Tang, J. W. Connor, and R. J. Hastie, "Kinetic-ballooning-mode theory in general geometry," Nucl. Fusion **20**(11), 1439 (1980).

[2]F. Zonca, L. Chen, and R. A. Santoro, "Kinetic theory of low-frequency Alfvén modes in tokamaks," Plasma Phys. Controlled Fusion **38**(11), 2011 (1996).
[3]J. W. Connor, R. J. Hastie, and J. B. Taylor, "Shear, periodicity, and plasma ballooning modes," Phys. Rev. Lett. **40**(6), 396–399 (1978).
[4]A. Hirose, L. Zhang, and M. Elia, "Higher order collisionless ballooning mode in tokamaks," Phys. Rev. Lett. **72**(25), 3993 (1994).
[5]A. Hirose and M. Elia, "Kinetic ballooning mode with negative shear[J]," Phys. review letters **76**(4), 628 (1996).
[6]A. Hirose and M. Elia, "Kinetic ballooning stability of internal transport barriers in tokamaks," Phys. Plasmas **10**(10), 1195–1198 (2003).
[7]I. Holod, D. Fulton, and Z. Lin, "Microturbulence in DIII-D tokamak pedestal. II. Electromagnetic instabilities," Nucl. Fusion **55**(9), 093020 (2015).
[8]Y. Chen, S. E. Parker, W. Wan, and R. Bravenec, "Benchmarking gyrokinetic simulations in a toroidal flux-tube," Phys. Plasmas (1994-present) **20**(9), 092511 (2013).
[9]A. Bottino, B. Scott, S. Brunner, B. F. McMillan, T. M. Tran, T. Vernay, L. Villard, S. Jolliet, R. Hatzky, and A. G. Peeters, "Global nonlinear electromagnetic simulations of tokamak turbulence," IEEE Trans. Plasma Sci. **38**(9), 2129–2135 (2010).
[10]A. Mishchenko, R. Hatzky, and A. Könies, "Global particle-in-cell simulations of Alfvénic modes[J]," Phys. Plasmas (1994-present) **15**(11), 112106 (2008).
[11]C. Bourdelle, W. Dorland, X. Garbet, G. W. Hammett, M. Kotschenreuther, G. Rewoldt, and E. J. Synakowski, "Stabilizing impact of high gradient of $\beta$ on microturbulence," Phys. Plasmas **10**(7), 2881–2887 (2003).
[12]E. A. Belli and J. Candy, "Fully electromagnetic gyrokinetic eigenmode analysis of high-beta shaped plasmas," Phys. Plasmas (1994–present) **17**(11), 112314 (2010).
[13]T. Görler, N. Tronko, W. A. Hornsby, A. Bottino, R. Kleiber, C. Norscini, V. Grandgirard, F. Jenko, and E. Sonnendrücker, "Intercode comparison of gyrokinetic global electromagnetic modes," Phys. Plasmas (1994–present) **23**(7), 072503 (2016).
[14]H. S. Xie, Y. Xiao, I. Holod, Z. Lin, and E. A. Belli, "Sensitivity of kinetic ballooning mode instability to tokamak equilibrium implementations," J. Plasma Phys. **82**(5) (2016).
[15]W. W. Lee, "Gyrokinetic approach in particle simulation," Phys. Fluids (1958-1988) **26**(2), 556–562 (1983).
[16]Z. Lin, T. S. Hahm, W. W. Lee, W. M. Tang, and R. B. White, "Turbulent transport reduction by zonal flows: Massively parallel simulations," Science **281**(5384), 1835–1837 (1998).
[17]Z. Lin and L. Chen, "A fluid–kinetic hybrid electron model for electromagnetic simulations]," Phys. Plasmas (1994–present) **8**(5), 1447–1450 (2001).
[18]Y. Xiao, I. Holod, Z. Wang, Z. Lin, and T. Zhang, "Gyrokinetic particle simulation of microturbulence for general magnetic geometry and experimental profiles," Phys. Plasmas (1994–present) **22**(2), 022516 (2015).
[19]I. Holod, W. L. Zhang, Y. Xiao, and Z. Lin, "Electromagnetic formulation of global gyrokinetic particle simulation in toroidal geometry," Phys. Plasmas (1994–present) **16**(12), 122307 (2009).
[20]J. A. C. Weideman, "Computation of the complex error function," SIAM J. Numer. Anal. **31**(5), 1497–1518 (1994).
[21]Ö. D. Gürcan, "Numerical computation of the modified plasma dispersion function with curvature," J. Comput. Phys. **269**, 156–167 (2014).
[22]W. Deng and Z. Lin, "Properties of microturbulence in toroidal plasmas with reversed magnetic shear," Phys. Plasmas (1994–present) **16**(10), 102503 (2009).
[23]L. Chen, A. Bondeson, and M. S. Chance, "Asymptotic stability boundaries of ballooning modes in circular tokamaks," Nucl. Fusion **27**(11), 1918 (1987).
[24]J. M. Greene and M. S. Chance, "The second region of stability against ballooning modes," Nucl. Fusion **21**(4), 453 (1981).